Journal of Solid State Chemistry 182 (2009) 484–490

Contents lists available at ScienceDirect

Journal of Solid State Chemistry

journal homepage: www.elsevier.com/locate/jssc

High-pressure synthesis and crystal structure of the mixed-valent titanium borate $Ti_5B_{12}O_{26}$

Almut Haberer, Hubert Huppertz *

Institut für Allgemeine, Anorganische und Theoretische Chemie, Leopold-Franzens-Universität Innsbruck, Innrain 52a, A-6020 Innsbruck, Austria

ARTICLE INFO

Article history:
Received 18 September 2008
Received in revised form
4 November 2008
Accepted 16 November 2008
Available online 3 December 2008

Keywords:
High-pressure
Multianvil
Crystal structure
Mixed-valent
Titanium borate

ABSTRACT

The new titanium borate was synthesized under high-pressure/high-temperature conditions in a Walker-type multianvil apparatus at 7.5 GPa and 1350 °C. $Ti_5B_{12}O_{26}$ is built up exclusively from corner-sharing BO_4-tetrahedra and shows a structural relation to the Zintl phase NaTl. Consisting of $B_{12}O_{26}$-clusters as fundamental building blocks, the structure of $Ti_5B_{12}O_{26}$ can be described via two interpenetrating diamond structures as in NaTl, where each atom corresponds to one $B_{12}O_{26}$-cluster. The tetragonal titanium borate crystallizes with eight formula units in the space group $I4_1/acd$ and exhibits lattice parameters of $a = 1121.1(2)$ pm and $c = 2211.5(4)$ pm. $Ti_5B_{12}O_{26}$ is a mixed-valent compound with Ti^{III} and Ti^{IV} cations. The environment of the titanium cations, as well as charge distribution calculations, leads us to the assumption that Ti^{III} and Ti^{IV} are located on different crystallographic sites.

1. Introduction

In the past years, studies of borates in high-pressure/high-temperature chemistry revealed a large variety of new compositions and polymorphs, for example the rare-earth oxoborates $RE_4B_6O_{15}$ (RE = Dy, Ho) [1–3], α-$RE_2B_4O_9$ (RE = Sm–Ho) [4–6], $Pr_4B_{10}O_{21}$ [7], and the *meta*-borates β-$RE(BO_2)_3$ (RE = La, Ce) [8,9]. Furthermore, a couple of new compositions could be realized in the compounds δ-SnB_4O_7 [10], CdB_2O_4 [11], and in a new non-centrosymmetric modification β-BiB_3O_6 of the well-characterized nonlinear optical material bismuth triborate [12]. In the last years, the transition metal borates were object of our research, yielding the compounds β-MB_4O_7 (M = Mn [13], Ni [13], Cu [13], Zn [14], Ca [15], Hg [16]), and the structurally exciting HP-NiB_2O_4, which consists solely of edge-sharing BO_4-tetrahedra [17]. In this context, we were also interested in the preparation of new titanium borates under extreme conditions of pressure and temperature.

Under ambient-pressure conditions, only two compositions have been known in the system Ti–B–O, i.e. $TiBO_3$ [18], crystallizing in the calcite structure, and the boron-containing rutile compound $TiB_{0.024}O_2$ [19]. So far, no high-pressure/high-temperature experiments have been reported for the titanium borate system. As $TiBO_3$ is the only titanium borate known until now, it is tempting to realize new Ti–B–O compounds under high-pressure conditions.

From titanium phosphates and titanium silicophosphates, several mixed-valent compounds are well acquainted, e.g. $MTi_3P_6Si_2O_{25}$ (M = K, Cs) [20], or the lazulite-type oxidephosphates $Ti^{III}Ti^{IV}_3O_3(PO_4)_3$ and $Ti^{III}_4Ti^{IV}_{27}O_{24}(PO_4)_{24}$ [21].

In this publication, we report the synthesis and the structural details of the first mixed-valent high-pressure titanium borate $Ti_5B_{12}O_{26}$.

2. Experimental section

The synthesis of the new titanium borate $Ti_5B_{12}O_{26}$ was carried out under high-pressure/high-temperature conditions, starting from the binary oxides TiO_2 and B_2O_3:

$$5\ TiO_2 + 6\ B_2O_3 \xrightarrow{7.5\ GPa,\ 1350\ °C} Ti_5B_{12}O_{26} + O_2 \quad (1)$$

A mixture of TiO_2 (anatase, ICDD 21-1272) and B_2O_3 (Strem Chemicals, Newburyport, USA, >99.9%) at a molar ratio of 5:6 (Eq. (1)) was ground up and filled into a boron nitride crucible (Henze BNP GmbH, HeBoSint® S10, Kempten, Germany). This crucible was placed into the center of an 18/11-assembly, which was compressed by eight tungsten carbide cubes (TSM-10 Ceratizit, Reutte, Austria). The details of preparing the assembly can be found in Refs. [22–26]. Pressure was applied by a multianvil device, based on a Walker-type module, and a 1000 ton press (both devices from the company Voggenreiter, Mainleus, Germany). The sample was compressed up to 7.5 GPa for 3 h, then heated to 1350 °C in 10 min and kept for 5 min.

* Corresponding author. Fax: +43 512 507 2934.
E-mail address: hubert.huppertz@uibk.ac.at (H. Huppertz).

0022-4596/$ - see front matter © 2008 Elsevier Inc. All rights reserved.
doi:10.1016/j.jssc.2008.11.022

Afterwards, the sample was cooled down to 950 °C in 15 min, followed by quenching to room temperature after switching off heating. Decompression required 9 h. The recovered experimental MgO-octahedron (pressure transmitting medium, Ceramic Substrates & Components Ltd., Newport, Isle of Wight, UK) was broken apart and the sample carefully separated from the surrounding boron nitride crucible, releasing the spherical black crystals of $Ti_5B_{12}O_{26}$, dispersed with colorless rutile, B_2O_3-II crystals, and amorphous B_2O_3. All attempts to gain a pure sample of $Ti_5B_{12}O_{26}$ failed; obviously, neither the applied temperature nor the reaction time sufficed for the full conversion of the educts.

Because $Ti_5B_{12}O_{26}$ comprises Ti^{III} and Ti^{IV} cations, the titanium cations from the starting material TiO_2 must be partly reduced from +IV to +III. From our experimental experience, we know about the reducing conditions in our high-pressure assembly, especially at high temperatures. Often, we observe that metallic impurities of corresponding metals of the oxides can be observed at the border of the crucible and in the sample, when the synthesizing temperature of a borate was too high. We suppose that the boron nitride of our crucible plays an important role in these reactions. Details about the mechanism of these reducing conditions are still unknown.

3. Crystal structure analysis

The sample was characterized by a powder diffraction pattern, which was obtained in transmission geometry from a flat sample of the reaction product, using a Huber Guinier powder diffractometer with Cu$K\alpha_1$ radiation (Ge monochromator, $\lambda = 154.06$ pm). Fig. 1 shows a typical powder pattern of the sample (top), exhibiting $Ti_5B_{12}O_{26}$, as well as rutile (the high-temperature phase of anatase), and the high-pressure phase B_2O_3-II [27] (arrows and lines). Due to the complexity of the powder pattern, the indexing of the titanium borate reflections failed. Additionally, the mount between 10° and 30° 2θ, which is caused by the amorphous part of the sample, aggravates the exact localization of the first reflections.

A single crystal of $Ti_5B_{12}O_{26}$ was isolated from the sample and examined through a Buerger precession camera, equipped with an image plate system (Fujifilm BAS-1800) in order to establish both, symmetry and suitability, for an intensity data collection. Intensity data were collected at room temperature by use of a Kappa CCD diffractometer (Bruker AXS/Nonius, Karlsruhe), equipped with a rotating Mo anode (graded multi-layer X-ray optics, $\lambda = 71.073$ pm). An absorption correction, based on multi-scans [28], was applied to the data set. All relevant details of the data collection and evaluation are listed in Table 1.

The structure solution and parameter refinement (full-matrix least-squares against F^2) were successfully performed, using the

Table 1
Crystal data and structure refinement of $Ti_5B_{12}O_{26}$.

Empirical formula	$Ti_5B_{12}O_{26}$
Molar mass (g/mol)	785.22
Crystal system	Tetragonal
Space group	$I4_1/acd$
Single crystal diffractometer	Kappa CCD
Radiation	Mo$K\alpha$ ($\lambda = 71.073$ pm)
Single crystal data	
a (pm)	1121.1(2)
c (pm)	2211.5(4)
Volume (Å^3)	2779.5(8)
Formula units per cell	$Z = 8$
Temperature (K)	293 (2)
Calculated density (g/cm^3)	3.753
Crystal size (mm^3)	$0.06 \times 0.05 \times 0.04$
Absorption coefficient (mm^{-1})	2.943
F(000)	3024
θ range (deg.)	$3.16 \leqslant \theta \leqslant 34.99$
Range in $h\,k\,l$	± 18, ± 18, ± 35
Total no. reflections	19229
Independent reflections	1533 ($R_{int} = 0.0422$)
Reflections with $I > 2\sigma(I)$	1341 ($R_\sigma = 0.0208$)
Data/parameters	1533/99
Absorption correction	Multi-scan (Scalepack [28])
Transm. ratio (min/max)	0.6218/0.7529
Goodness-of-fit (F^2)	1.182
Final R indices ($I > 2\sigma(I)$)	$R_1 = 0.0302$
	w$R_2 = 0.0759$
R indices (all data)	$R_1 = 0.0355$
	w$R_2 = 0.0779$
Largest differ. peak, deepest hole (e/Å^3)	1.21/−0.81

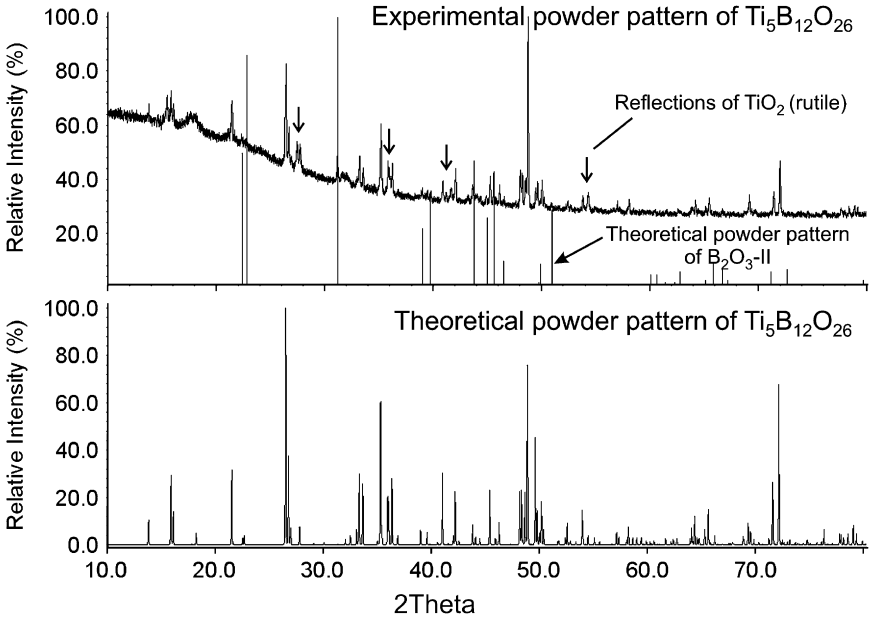

Fig. 1. *Top*: Experimental powder pattern of $Ti_5B_{12}O_{26}$; reflections of the high-pressure phase B_2O_3-II [27] (lines) and the high-temperature phase of TiO_2 (rutile, arrows) are indicated. *Bottom*: Theoretical powder pattern of $Ti_5B_{12}O_{26}$, based on single-crystal diffraction data.

SHELX-97 software suite [29,30] with anisotropic atomic displacement parameters for all atoms. According to the systematic extinctions, the tetragonal space group $I4_1/acd$ (no. 142) was derived. The final difference Fourier syntheses did not reveal any significant residual peaks in all refinements. The positional parameters of the refinements, anisotropic displacement parameters, interatomic distances, and interatomic angles are listed in Tables 2–5. Further information of the crystal structure is available from the Fachinformationszentrum Karlsruhe (crysdata@fiz-karlsruhe.de), D-76344 Eggenstein-Leopoldshafen (Germany), by quoting the Registry No. CSD-419876.

4. Results and discussion

The structure of $Ti_5B_{12}O_{26}$ is built up exclusively of corner-sharing BO_4-tetrahedra. Fig. 2 depicts the formation of $B_{12}O_{26}$-clusters from four of the smallest building block units B_3O_9. These $B_{12}O_{26}$-clusters are connected with each other to build up a structure very closely related to the structure of the known Zintl phase NaTl [31] (Fig. 3), which consists of two interpenetrating diamond structures. Fig. 4 shows the structural features of $Ti_5B_{12}O_{26}$, compared with the analogous fragments of the NaTl structure. The atomic positions, filled with Na^+ and Tl^- ions in NaTl, are now occupied by $B_{12}O_{26}$-clusters in $Ti_5B_{12}O_{26}$, which leads to a tetrahedral connection of each $B_{12}O_{26}$-cluster with four other clusters (Fig. 4, top and right). Corresponding to the cationic and anionic diamond structures in NaTl, there are two independent $B_{12}O_{26}$-cluster networks, not connected by B–O bonds (Fig. 4, bottom). The cluster types in the two networks simply differ through the orientation of their tetrahedra.

Fig. 5 gives a view of the crystal structure along the body diagonal [111]. Titanium cations are positioned in channels, which run along [111] and between the clusters. Interestingly, there are not any titanium ions inside the clusters, leaving a large octahedral cavity (Fig. 2). Viewing along [010] (Fig. 6), rectangular channels are visible, which are also empty.

The B–O bond-lengths in the BO_4-tetrahedra of $Ti_5B_{12}O_{26}$ (Table 4) vary between 144.7 and 150.9 pm with an average B–O bond-length of 148.2 pm, which tallies well to the known average

Table 4
Interatomic distances (pm) in $Ti_5B_{12}O_{26}$, calculated with the single-crystal lattice parameters.

Ti1–O3a	195.0(2)	Ti2–O6	207.3(2)(2 ×)
Ti1–O3b	196.1(1)	Ti2–O7	219.5(1)(4 ×)
Ti1–O1	201.1(1)		∅ = 215.4
Ti1–O2	201.2(1)		
Ti1–O5	204.7(2)		
Ti1–O4	211.0(1)		
	∅ = 201.5		
B1–O2	147.7(2)	B2–O1	148.3(2)
B1–O3	144.7(2)	B2–O4	149.0(2)
B1–O5	148.3(2)	B2–O5	148.7(2)
B1–O7	150.3(2)	B2–O6	146.8(2)
	∅ = 147.8		∅ = 148.2
B3–O1	148.4(2)		
B3–O2	147.1(2)		
B3–O4	150.9(2)		
B3–O7	148.2(2)		
	∅ = 148.7		

Table 2
Atomic coordinates and isotropic equivalent displacement parameters (U_{eq}/Å^2) for $Ti_5B_{12}O_{26}$ (space group: $I4_1/acd$). U_{eq} is defined as one-third of the trace of the orthogonalized U_{ij} tensor.

Atom	*Wyckoff* site	*x*	*Y*	*z*	U_{eq}
Ti1	32*g*	0.34191(2)	0.07007(2)	0.04252(1)	0.00689(8)
Ti2	8*b*	1/2	1/4	7/8	0.0083(1)
B1	32*g*	0.4063(2)	0.4835(2)	0.08254(6)	0.0072(2)
B2	32*g*	0.4119(2)	0.3224(2)	0.00130(6)	0.0072(2)
B3	32*g*	0.2547(2)	0.3161(2)	0.08251(6)	0.0076(2)
O1	32*g*	0.33602(9)	0.24931(9)	0.04183(4)	0.0067(2)
O2	32*g*	0.32723(9)	0.40225(9)	0.11664(4)	0.0070(2)
O3	32*g*	0.33263(9)	0.56001(8)	0.04541(4)	0.0069(2)
O4	32*g*	0.33726(8)	0.38203(9)	0.095445(4)	0.0068(2)
O5	32*g*	0.47673(9)	0.40947(9)	0.03994(4)	0.0073(2)
O6	16*d*	1/2	1/4	0.96873(6)	0.0064(2)
O7	32*g*	0.48505(9)	0.55477(9)	0.12398(4)	0.0069(2)

Ti^{III} and Ti^{IV} can presumably be assigned to Ti1 and Ti2, respectively.

Table 3
Anisotropic displacement parameters (U_{ij}/Å^2) for $Ti_5B_{12}O_{26}$ (space group: $I4_1/acd$).

Atom	U_{11}	U_{22}	U_{33}	U_{12}	U_{13}	U_{23}
Ti1	0.0071(2)	0.0071(2)	0.0065(2)	−0.00036(7)	0.00032(7)	−0.00058(7)
Ti2	0.0094(2)	0.0094(2)	0.0062(2)	0	0	0.0010(2)
B1	0.0073(5)	0.0078(6)	0.0066(6)	−0.0002(4)	−0.0001(4)	−0.0003(4)
B2	0.0066(5)	0.0076(5)	0.0074(5)	0.0003(4)	0.0007(4)	0.0005(4)
B3	0.0069(5)	0.0080(6)	0.0078(5)	0.0001(4)	0.0005(4)	0.0001(4)
O1	0.0074(4)	0.0058(4)	0.0068(4)	0.0004(3)	0.0012(3)	0.0015(3)
O2	0.0077(4)	0.0073(4)	0.0060(4)	−0.0003(3)	0.0003(3)	−0.0011(3)
O3	0.0076(4)	0.0066(4)	0.0066(4)	0.0010(3)	0.0004(3)	0.0008(3)
O4	0.0069(4)	0.0065(4)	0.0069(4)	−0.0001(3)	−0.0013(3)	0.0001(3)
O5	0.0066(4)	0.0078(4)	0.0075(4)	−0.0020(3)	−0.0003(3)	−0.0005(3)
O6	0.0067(5)	0.0077(5)	0.0049(5)	0	0	0.0020(4)
O7	0.0070(4)	0.0070(4)	0.0068(4)	−0.0001(3)	−0.0019(3)	−0.0006(3)

Table 5
Interatomic angles (deg.) in $Ti_5B_{12}O_{26}$, calculated with the single-crystal lattice parameters.

O3–B1–O2	108.3(2)	O6–B2–O1	112.1(1)	O2–B3–O7	108.6(1)
O3–B1–O5	106.0(1)	O6–B2–O5	108.4(1)	O2–B3–O1	107.6(2)
O2–B1–O5	107.4(1)	O1–B2–O5	107.2(1)	O7–B3–O1	111.2(2)
O3–B1–O7	111.5(2)	O6–B2–O4	106.5(1)	O2–B3–O4	109.5(2)
O2–B1–O7	111.7(2)	O1–B2–O4	110.3(2)	O7–B3–O4	110.2(1)
O5–B1–O7	111.8(2)	O5–B2–O4	112.3(2)	O1–B3–O4	109.8(1)
	∅ = 109.5		∅ = 109.5		∅ = 109.5

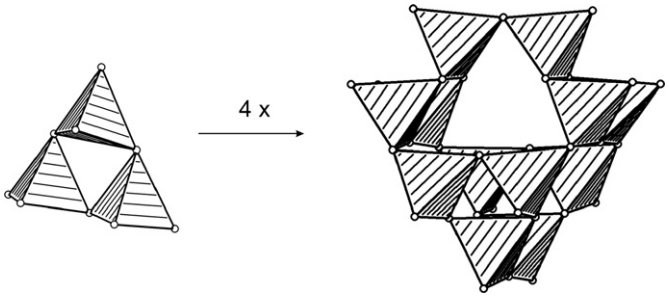

Fig. 2. Formation of $B_{12}O_{26}$-clusters from the fundamental building block B_3O_9, depicting the large octahedral cavity inside the $B_{12}O_{26}$-cluster.

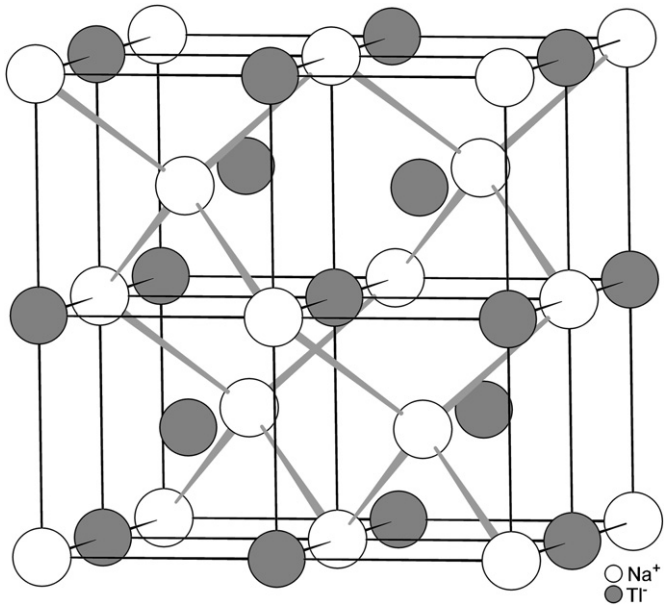

Fig. 3. The NaTl structure.

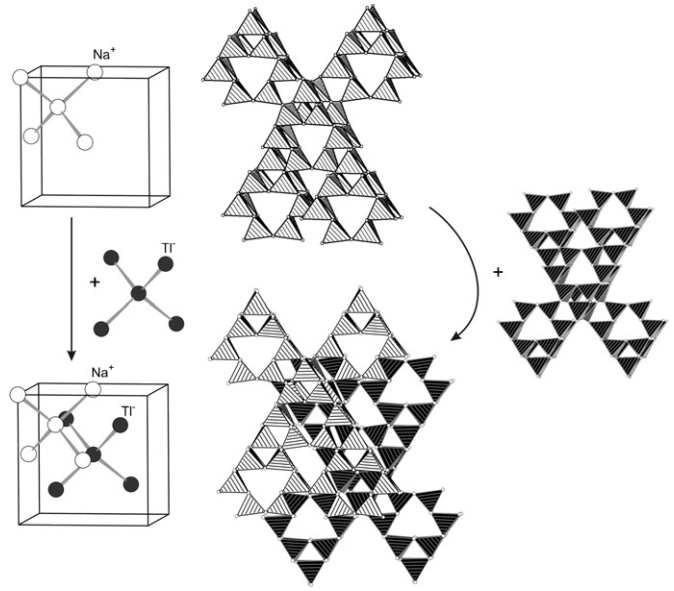

Fig. 4. *Top*: Tetrahedral connection of $B_{12}O_{26}$-clusters (center), compared with the corresponding unit in the NaTl structure (left). *Right*: The second diamond analogous network consists of $B_{12}O_{26}$-clusters with different orientation. *Bottom*: Combination of the two networks (center) and the corresponding unit in the NaTl structure (left).

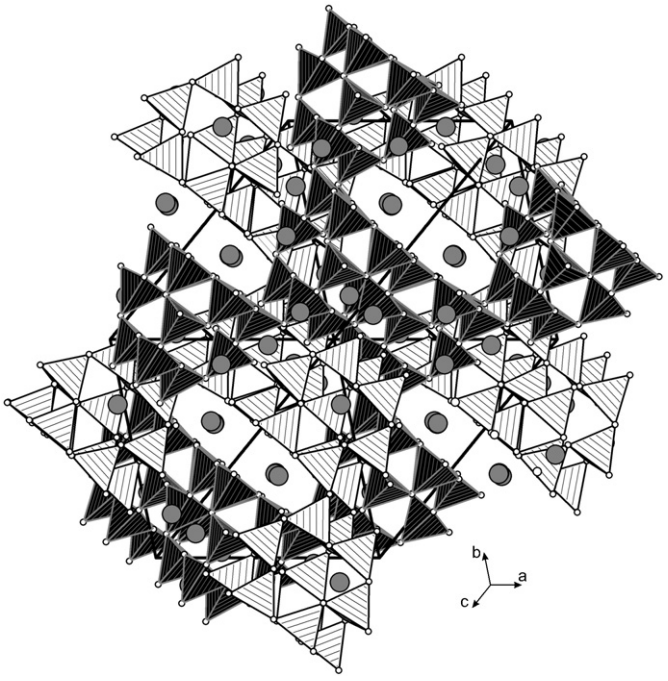

Fig. 5. Crystal structure of $Ti_5B_{12}O_{26}$; view along [111]. Titanium cations are located in channels, that run along the body diagonal (Ti: dark grey spheres; O: open spheres).

value of 147.6 pm for BO_4-tetrahedra in borates [32,33]. The O–B–O angles in the three crystallographically independent BO_4-tetrahedra range between 106.0° and 112.3° (Table 5) with a mean value of 109.5°.

Two crystallographically different titanium cations Ti1 and Ti2 were found in $Ti_5B_{12}O_{26}$ (Table 2). In order to gain a charge balanced $Ti_5B_{12}O_{26}$, we need a mixed-valent distribution of titanium cations, where four-fifth of the titanium cations must be Ti^{III}, while one-fifth remains Ti^{IV}. According to the titanium sites listed in Table 2, this would easily be achieved by assigning Ti1 (32*g*) and Ti2 (8*b*) to Ti^{III} and Ti^{IV}, respectively.

Both titanium ions are sixfold-coordinated by oxygen, showing distorted octahedral coordinations (Fig. 7). While the Ti2–O octahedron is isolated, two Ti1–O octahedrons are connected via one common edge. This results in a fairly short Ti1–Ti1 distance of 278.98(6) pm (in titanium metal, Ti–Ti distances average 286 pm [34]). The linkage of Ti^{IV}–O octahedra via edges is commonly found, e.g. in the different modifications of TiO_2. Nevertheless, it seems unlikely for highly charged ions to be found in such close proximity, since the Ti–Ti distances in rutile (295.3(1) pm) [35], brookite (306.3(3) and 297.6(3) pm) [36], and anatase (303.6(2) pm) [37] are noticeably larger. We take this as another

hint for Ti^{III}, occupying the Ti1 position, due to the lesser cation–cation repulsion.

Considering the Ti–O bond-lengths in Table 4, the distances Ti1–O are close to the value of 206.4(1) pm, found for Ti^{III} in $TiBO_3$ [18]. The Ti2–O bond-lengths are significantly larger, which is disturbing, when Ti2 is assigned as the highly charged Ti^{IV}. An explanation of this fact might be a second-order Jahn–Teller effect, which has been reported for octahedrally coordinated d^0 cations [38]. Due to the small ionic radius and the high charge of the atom, empty *d*-orbitals are energetically lowered, which results in an overlap of those orbitals with the filled *p*-orbitals of the ligands. In a solid-state compound, this generates a multitude of nearly identical electronic configurations. As in the classical Jahn–Teller effect, these degenerated states are suspended by the lowering of symmetry, leading to an energetically more favourable state. A distortion of the octahedral coordination sphere around Ti^{IV} cations is frequently reported from many titanium oxides, leading to shortened and elongated Ti–O distances up to 220 pm [39].

The calculations of the bond-valence sums for $Ti_5B_{12}O_{26}$ were performed by applying the bond-length/bond-strength (ΣV) and the CHARDI concept (ΣQ) (Table 6) [40–42]. Whilst the CHARDI results of +3.04 for Ti1 and +3.69 for Ti2 confirm our assignment of the titanium cations pretty well, the bond-valence sums ΣV lead to strange charge values, especially for Ti2. Presumably, the bond-length/bond-strength concept failed because of the very long Ti–O bonds, evoked by the Jahn–Teller distortion. On the other hand, CHARDI calculates a value of −2.41 for O6, which is far

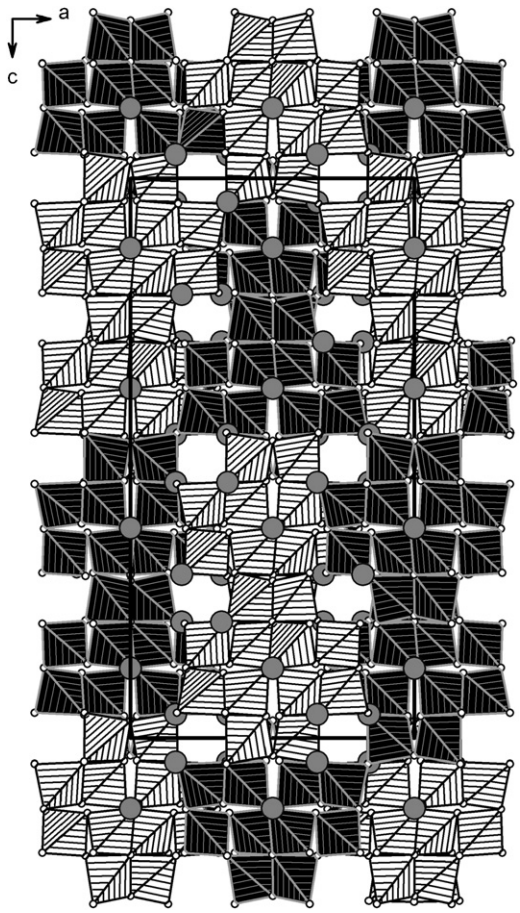

Fig. 6. Crystal structure of $Ti_5B_{12}O_{26}$; view along [010] (Ti: dark grey spheres, O: open spheres).

Table 6
Charge distribution in $Ti_5B_{12}O_{26}$, calculated with the bond-length/bond-strength concept (ΣV) [40,41] and the CHARDI concept (ΣQ) [42].

	Ti1	Ti2	B1	B2	B3		
ΣQ	3.04	3.69	2.99	2.99	3.06		
ΣV	3.31	2.43	3.00	2.97	2.93		
	O1	O2	O3	O4	O5	O6	O7
ΣQ	−2.01	−2.05	−2.03	−1.77	−1.92	−2.41	−2.03
ΣV	−2.03	−2.06	−2.10	−1.88	−1.85	−2.04	−1.80

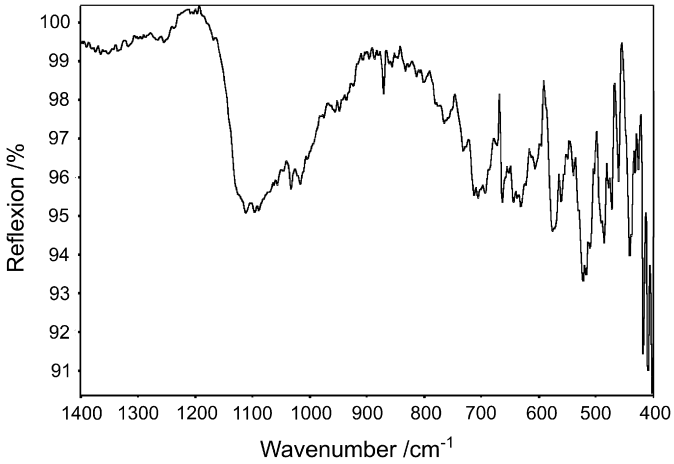

Fig. 8. IR-spectrum of the reaction products $Ti_5B_{12}O_{26}$ and TiO_2 (rutile).

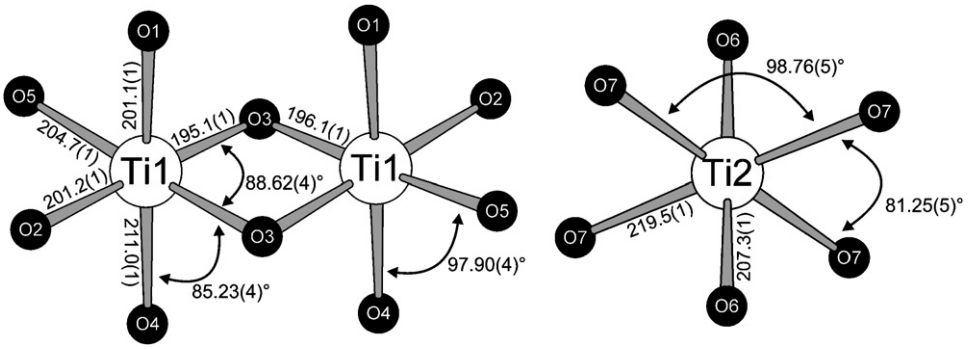

Fig. 7. Coordination spheres of the titanium ions. Ti^{III} and Ti^{IV} can presumably be assigned to Ti1 and Ti2, respectively. Ti–O distances are shown in pm.

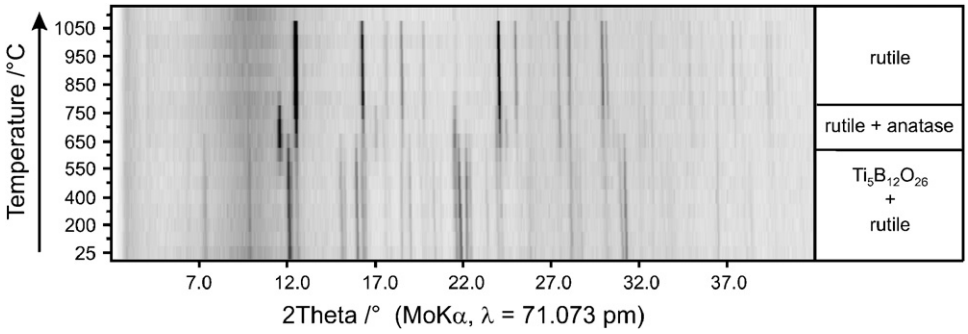

Fig. 9. *In-situ* temperature-programmed X-ray powder diffraction patterns, showing the decomposition of $Ti_5B_{12}O_{26}$ at 600 °C.

too negative. Here, the result of the bond-length/bond-strength calculation with a value of −2.04 tallies well with the expected value of −2.

Furthermore, we calculated the Madelung Part of Lattice Energy (MAPLE) values [43–45] for $Ti_5B_{12}O_{26}$ in order to compare them with the MAPLE values of the binary components TiO_2 (rutile) [46], Ti_2O_3 [47], and the high-pressure modification B_2O_3-II [27]. The additive potential of the MAPLE values allows the calculation of hypothetical values for $Ti_5B_{12}O_{26}$, starting from binary oxides. As a result, we obtained a value of 178295 kJ/mol in comparison to 178971 kJ/mol (deviation: 0.4%), starting from the binary oxides [1 TiO_2 (13625 kJ/mol) + 2 Ti_2O_3 (16859 kJ/mol) + 6 B_2O_3-II (21938 kJ/mol)].

5. IR spectroscopy

The infrared spectrum of $Ti_5B_{12}O_{26}$ was recorded on a Nicolet 5700 FT-IR spectrometer, scanning a range from 400 to 4000 cm^{-1}. Before the measurement, the sample was thoroughly dried under high vacuum for several days. Fig. 8 shows the spectral region between 400 and 1400 cm^{-1}. The absorption peaks between 790 and 1150 cm^{-1} are those typical for the tetrahedral borate group $[BO_4]^{5-}$ as in π-$GdBO_3$, π-YBO_3, or $TaBO_4$ [48–50]. Below 700 cm^{-1}, absorptions of TiO_2 can be found. They agree well with the rutile absorption curve in the database of the NIST Chemical WebBook [51]. In the region of 3000–3500 cm^{-1} (not displayed in Fig. 8), no absorption peaks could be detected. Peaks at those wavelengths can be assigned to OH groups and would be typical for water-containing borates. On the basis of this IR measurement, we can exclude the presence of OH groups in $Ti_5B_{12}O_{26}$.

6. Thermal behavior

The *in-situ* temperature-programmed X-ray powder diffraction experiment was performed in air on a STOE Stadi P powder diffractometer (Mo*K*α radiation, $\lambda = 71.073$ pm) with a computer-controlled STOE furnace. The sample was enclosed in a quartz capillary and heated from room temperature up to 500 °C in steps of 100°, and from 500 to 1100 °C in steps of 50°. The capillary broke at 1100 °C, so no data were obtained while cooling the sample down to room temperature. At each temperature step, a diffraction pattern was recorded over the angular range $2° \leqslant 2\theta \leqslant 47°$. Fig. 9 shows that the reflections of $Ti_5B_{12}O_{26}$ start to fade at 600 °C and are undetectable at 700 °C. Above 600 °C, reflections of anatase become visible, leading to the assumption that $Ti_5B_{12}O_{26}$ decomposes at that temperature, forming anatase and amorphous boron oxide (not visible in the XRD diagram) as decomposition products. At 800 °C, anatase is completely transformed to rutile, which can be seen in the latter's darker reflection lines. The transition of anatase to rutile at high temperatures is commonly known; due to the preparation of the TiO_2 compound, transition temperatures can vary between 350 and 1175 °C [52].

7. Conclusions

In this article, we described the synthesis, crystal structure, and thermal properties of the new high-pressure phase $Ti_5B_{12}O_{26}$. It is the first known mixed-valent titanium borate and crystallizes in a structure closely related to the Zintl phase NaTl. Large cavities inside the $B_{12}O_{26}$-clusters and a network of channels through the structure could be an indication for interesting physical properties of $Ti_5B_{12}O_{26}$. Due to the investigations and calculations presented in this paper, we presume that the titanium cations Ti^{III} and Ti^{IV} can be assigned to the different crystallographic sites 32*g* and 8*b*, respectively. The synthesis of pure $Ti_5B_{12}O_{26}$ starting from educts with titanium in different oxidation states and measurements concerning other physical properties will be object of further investigations.

Acknowledgments

We thank Thomas Miller (LMU München) for collecting the single-crystal and HT-XRD data. Special thanks go to Prof. Dr. D. Johrendt for measurements at the Huber Guinier powder diffractometer and to Prof. Dr. W. Schnick (LMU München) for his continuous support of these investigations. This work was financially supported by the Deutsche Forschungsgemeinschaft (HU 966/2-3) and the Fonds der Chemischen Industrie.

References

[1] H. Huppertz, B. von der Eltz, J. Am. Chem. Soc. 124 (2002) 9376.
[2] H. Huppertz, Z. Naturforsch. B58 (2003) 278.
[3] H. Huppertz, H. Emme, J. Phys.: Condens. Matter 16 (2004) 1283.
[4] H. Emme, H. Huppertz, Z. Anorg. Allg. Chem. 628 (2002) 2165.
[5] H. Emme, H. Huppertz, Chem. Eur. J. 9 (2003) 3623.
[6] H. Emme, H. Huppertz, Acta Crystallogr. C61 (2005) i29.
[7] A. Haberer, G. Heymann, H. Huppertz, J. Solid State Chem. 180 (2007) 1595.
[8] G. Heymann, T. Soltner, H. Huppertz, Solid State Sci. 8 (2006) 821.
[9] A. Haberer, G. Heymann, H. Huppertz, Z. Naturforsch. B62 (2007) 759.
[10] J.S. Knyrim, F.M. Schappacher, R. Pöttgen, J. Schmedt auf der Günne, D. Johrendt, H. Huppertz, Chem. Mater. 19 (2007) 254.
[11] J.S. Knyrim, H. Emme, M. Döblinger, O. Oeckler, M. Weil, H. Huppertz, Chem. Eur. J. 19 (2008) 6149.
[12] J.S. Knyrim, P. Becker, D. Johrendt, H. Huppertz, Angew. Chem. 118 (2006) 8419;
J.S. Knyrim, P. Becker, D. Johrendt, H. Huppertz, Angew. Chem. Int. Ed. 45 (2006) 8239.
[13] J.S. Knyrim, J. Friedrichs, S. Neumair, F. Roeßner, Y. Floredo, S. Jakob, D. Johrendt, R. Glaum, H. Huppertz, Solid State Sci. 10 (2007) 168.
[14] H. Huppertz, G. Heymann, Solid State Sci. 5 (2003) 281.
[15] H. Huppertz, Z. Naturforsch. B58 (2003) 257.
[16] H. Emme, M. Weil, H. Huppertz, Z. Naturforsch. B60 (2005) 815.

[17] J.S. Knyrim, F. Roeßner, S. Jakob, D. Johrendt, I. Kinski, R. Glaum, H. Huppertz, Angew. Chem. 119 (2007) 9256;
J.S. Knyrim, F. Roeßner, S. Jakob, D. Johrendt, I. Kinski, R. Glaum, H. Huppertz, Angew. Chem. Int. Ed. 46 (2007) 9097.
[18] M. Huber, H.J. Deiseroth, Z. Kristallogr. 210 (1995) 685.
[19] I.E. Grey, C. Li, C.M. MacRae, L.A. Bursill, Solid State Sci. 127 (1996) 240.
[20] A. Benmoussa, M.M. Borel, A. Grandin, A. Leclaire, B. Raveau, Acta Crystallogr. C47 (1991) 936.
[21] M. Schoeneborn, R. Glaum, F. Reichenauer, J. Solid State Chem. 181 (2008) 1367.
[22] D. Walker, M.A. Carpenter, C.M. Hitch, Am. Mineral. 75 (1990) 1020.
[23] D. Walker, Am. Mineral. 76 (1991) 1092.
[24] H. Huppertz, Z. Kristallogr. 219 (2004) 330.
[25] D.C. Rubie, Phase Transitions 68 (1999) 431.
[26] N. Kawai, S. Endo, Rev. Sci. Instrum. 8 (1970) 1178.
[27] C.T. Prewitt, R.D. Shannon, Acta Crystallogr. B24 (1968) 869.
[28] Z. Otwinowski, W. Minor, Methods Enzymol. 276 (1997) 307.
[29] G.M. Sheldrick, SHELXS-97 and SHELXL-97, Program Suite for the Solution and Refinement of Crystal Structures, University of Göttingen, Göttingen, Germany, 1997.
[30] G.M. Sheldrick, Acta Crystallogr. A64 (2008) 112.
[31] E. Zintl, W. Dullenkopf, Z. Phys. Chem. B16 (1932) 195.
[32] F.C. Hawthorne, P.C. Burns, J.D. Grice, Reviews in mineralogy, in: Boron: Mineralogy, Petrology, and Geochemistry, vol. 33, Mineralogical Society of America, Washington, DC, 1996 (Chapter 2).
[33] E. Zobetz, Z. Kristallogr. 191 (1990) 45.
[34] E. Riedel, Moderne Anorganische Chemie, 2. Auflage, de Gruyter-Verlag, Berlin, New York, 2003, 446pp.
[35] C. Legrand, J. Delville, Golden Book of Phase Transitions 1, Wroclaw, 2002, 1pp.
[36] E.P. Meagher, G.A. Lager, Can. Mineral. 17 (1979) 77.
[37] D.T. Cromer, K. Herrington, J. Am. Chem. Soc. 77 (1955) 4708.
[38] M. Kunz, I.D. Brown, J. Solid State Chem. 115 (1995) 395.
[39] M. Gasperin, Acta Crystallogr. B31 (1975) 2129.
[40] I.D. Brown, D. Altermatt, Acta Crystallogr. B41 (1985) 244.
[41] N.E. Brese, M. O'Keeffe, Acta Crystallogr. B47 (1991) 192.
[42] R. Hoppe, S. Voigt, H. Glaum, J. Kissel, H.P. Müller, K.J. Bernet, Less-Common Met. 156 (1989) 105.
[43] R. Hoppe, Angew. Chem. 78 (1966) 52;
R. Hoppe, Angew. Chem. Int. Ed. 5 (1966) 96.
[44] R. Hoppe, Angew. Chem. 82 (1970) 7;
R. Hoppe, Angew. Chem. Int. Ed. 9 (1970) 25.
[45] R. Hübenthal, MAPLE—Program for the Calculation of MAPLE Values, Vers. 4, University of Gießen, Gießen, Germany, 1993.
[46] W.H. Baur, Acta Crystallogr. 9 (1956) 515.
[47] R.E. Newnham, Y.M. de Haan, Z. Kristallogr. Kristallgeom. Kristallphys. Kristallchem. 117 (1962) 235.
[48] M. Ren, J.H. Lin, Y. Dong, L.Q. Yang, M.Z. Su, L.P. You, Chem. Mater. 11 (1999) 1576.
[49] J.P. Laperches, P. Tarte, Spectrochim. Acta 22 (1966) 1201.
[50] G. Blasse, G.P.M. van den Heuvel, Phy. Status Solidi 19 (1973) 111.
[51] Coblentz Society, Inc., Evaluated Infrared Reference Spectra, in: P.J. Linstrom, W.G. Mallard (Eds.), NIST Chemistry WebBook, NIST Standard Reference Database Number 69, June 2005, National Institute of Standards and Technology, Gaithersburg MD, 20899, 〈http://webbook.nist.gov〉.
[52] A. Daffier, A. Feltz, J. Jung, W. Ludwig, E. Kaisersberger, J. Thermal Anal. 33 (1988) 803.